Nuclear Engineering and Design 136 (1992) 243–254
North-Holland



# Axial crack propagation in fuel pin cladding tubes

I.J. Ford

*Theoretical Studies Department, AEA Industrial Technology, B424.4, Harwell Laboratory, Didcot, Oxon, OX11 0RA, United Kingdom*

Received 2 January 1992, revised version 21 April 1992

We describe a mechanistic approach to the modelling of the propagation of an axial crack in the wall of a cladding tube and its use in analysing nuclear fuel pin rupture in accident conditions. An energy flow analysis is used to calculate the crack propagation velocity, balancing work done by the pin internal pressure against energy dissipated through plastic deformation and other mechanisms. An initial crack length is used based on experimental observation, and assuming steady state propagation is set up immediately. The arrest of the crack occurs when the pin becomes sufficiently depressurised. A simple criterion for this is proposed, based on ideas of gassy molten fuel pressurisation, a mechanism relevant to fuel pin rupture. A numerical model of the process of axial crack propagation and arrest is described.

## 1. Introduction

The modelling of various failure processes for irradiated steels has recently been described and applied to the prediction of nuclear fuel pin failure [1,2]. We now consider the axial propagation of a crack in the cladding tube, which follows the initial fracture. Our approach, as before, is to construct models based on a mechanistic understanding of the processes occurring, rather than attempting to formulate some kind of empirical correlation. It is expected that a mechanistic model is better able to describe processes outside the original experimental database than a set of empirical rules, and also ways of improving the modelling, where necessary, are clearer.

Predicting the propagation of a fuel pin failure is in some situations as important as obtaining the correct timing and location of the initial failure. This is because in whole core fast reactor accident analysis, the post-failure motion of fuel can strongly affect the subsequent development of the accident, either towards an early termination or an escalation of the incident. This is due to changes in reactivity, and therefore fission energy release, arising from changes in fuel geometry. To be precise, we refer to propagation as the initial, normally very fast, axial extension of the cladding crack away from the failure position. Escape of fuel material from the pin reduces the internal pressure which arrests the propagation. We limit ourselves here to a discussion of the initial, mechanical crack propagation and seek to provide a single prediction: the axial length of the rupture.

*Correspondence to:* Dr. I.J. Ford, Theoretical Studies Department, AEA Industrial Technology, B424.4, Harwell Laboratory, Didcot, Oxon, OX11 0RA, United Kingdom.

## 2. Axial rip propagation

### 2.1. Energy balance

There are three aspects of a calculation of axial crack propagation which need to be considered: the initial crack length, the velocity of propagation, and an arrest condition. The most straightforward to address is the estimation of velocity, under the assumption that a quasi-steady state situation has been set up. An analysis of the balance of the supply of energy to the cladding, and its dissipation, can in principle yield the propagation velocity of a running crack. In practice, however, assumptions have to be made concerning the geometry of the crack, since plastic deformation is important but a full elasto-plastic deformation solution to the problem is not available. (An elastic solution is available [3,4], but is not adequate as plastic strains of the order of 1% are expected, compared to typical elastic strains of 0.1%).

Elsevier Science Publishers B.V.

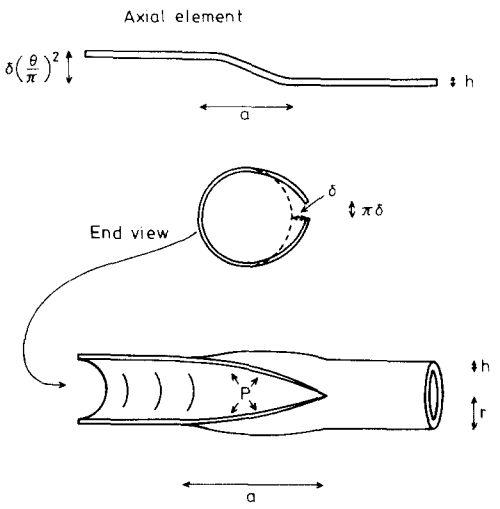


Fig. 1. Geometry of an axial crack in a cladding tube.

The following parametrisation of the rip geometry has been used [5]: the radial displacement of the cladding tube is

$$w(z,\theta)=\begin{cases}0 & z<0,\\ \delta\sin^2\left(\dfrac{\pi z}{2a}\right)\left(\dfrac{\theta}{\pi}\right)^2 & 0<z<a,\\ \delta\left(\dfrac{\theta}{\pi}\right)^2 & z>a,\end{cases}$$

where $z$ is the axial coordinate and $\theta$ the azimuthal angle. The origin moves with the tip of the crack. The crack edges lie along $\theta=\pm\pi$ and $\delta$ is the maximum radial displacement. For $z>a$ all deformation has ceased: $a$ is the crack tip length. Figure 1 illustrates the deformation of the cladding tube. Our parametrisation has the advantage that the deformation is smooth: other choices used by Freund and Parks [6] and Poynton [7] involve sharp bends.

We now can discuss the various terms in the energy flow equation. The main driving force is the pin internal pressure, which does work on the clad in deforming it into the cracked geometry. If we assume that the pressure $P$ is not reduced by the action of pushing out the clad, and does not vary across the crack flaps, then the rate of addition of energy is

$$\dot{W}=\int_0^a\int_{-\pi}^{\pi} r\,\mathrm{d}z\,\mathrm{d}\theta\dot{w}(z,\theta)P, \tag{1}$$

where $r$ is the cladding tube radius, shown in fig. 1. In all our work, $P$ represents the difference in pressure between the inside and outside of the clad, but will be referred to as the internal pressure.

Instead of evaluating the time derivative $\dot{w}$ we shall use a consistent convention that the energy inputs or losses corresponding to the deformed geometry occur over a time interval $a/v$, where $v$ is the crack propagation velocity. Hence $\dot{W}$ is given by

$$\dot{W}=\int_0^a\int_{-\pi}^{\pi} r\,\mathrm{d}z\,\mathrm{d}\theta w(z,\theta)Pv/a=\frac{\pi}{3}BvraP, \tag{2}$$

where we have introduced the crack shape parameter $B=\delta/a$.

A second source of energy is from the relaxation of elastic stresses following the fracture. This energy resides in the unfractured cladding with a density $\sigma_\theta^2/(2E)$ where $\sigma_\theta$ is the hoop stress ($\approx Pr/h$ where $h$ is the clad wall thickness) and $E$ is Young's modulus. The rate of supply of this energy is then

$$\dot{A}=\int_0^a\int_{-\pi}^{\pi} r\,\mathrm{d}z\,\mathrm{d}\theta\frac{h\sigma_\theta^2}{2E}\frac{v}{a}=\pi rhv\frac{\sigma_\theta^2}{E}. \tag{3}$$

On the energy dissipation side we have to consider at least three mechanisms: the most straightforward is the fracture work rate. This is the energy required to create fracture surface, and arises fundamentally from the breaking of atomic bonds and local deformation close to the fracture surface. The rate of energy dissipation is

$$\dot{F}=\frac{K^2}{E}ahv/a=\frac{K^2}{E}hv, \tag{4}$$

where $K$ is the fracture toughness. While data exist for $K$ as a function of temperature for both fresh and irradiated 20% cw AISI 316 steel [8] the situation is complicated by the relative thinness of the cladding. Fits to $K$, in MPa $\mathrm{m}^{1/2}$, can be written

$$K=(70(T-473)+130(973-T))/500, \tag{5}$$

for fresh cladding and

$$K=(40(T-473)+90(973-T))/500, \tag{6}$$

for irradiated cladding, both for the range 473 K $<T<$ 973 K, [8] but these would apply subject to a thickness condition $h\gg h_0=K^2/(3\pi\sigma_y^2)$ (which is to say the plastic zone at the crack tip is much smaller than the clad thickness: $\sigma_y$ is the yield stress). The length $h_0$ is typically several cm whilst the clad thickness is usually about 0.5 mm, so alterations to the above expressions are necessary, due to the plane stress conditions cre-

ated (radially) in thin clad in contrast to the plane strain conditions necessary for the validity of eqns (5) and (6). The appropriate fracture toughness will be greater than the data in [8] would suggest. Models for this effect have been proposed, one of which [9,10] suggests the form

$$K(h) = K(h \to \infty)\left(1 + \frac{\epsilon_f \sigma_y}{24E} h_0/h\right)^{1/2}, \tag{7}$$

for $h > h_0$, and $K = K(h_0)$ for $h < h_0$. $\epsilon_f$ is the failure strain. However, these models have had poor success in explaining the data. The situation is rather unclear, but fortunately this will not greatly affect our final conclusions.

Secondly we have energy dissipation from gross plastic deformation of the tube. It is easy to see that this can be separated, to an approximation, into two parts: azimuthal bending and axial bending. The first of these is permanent and leaves the cladding tube cross-section deformed into a U-shape. Axial bending, however, involves forcing straight axial elements of the tube wall through an S-shape over the crack tip length $a$. The deformation is not permanent since the final shape of the axial element is again straight, as can be seen in fig. 1. (Since the deformation is not permanent there exists the possibility that the bending can occur elastically, or partly so, which does not involve as much dissipation of energy, and indeed the stored elastic energy is returned when the deformation is reversed. We shall return to this point again shortly.)

The plastic work associated with giving a straight rod a radius of curvature $\rho$ has a density

$$\Gamma(z, \theta) = \frac{\sigma_y h}{4\rho}, \tag{8}$$

assuming no work hardening. The azimuthal radius of curvature for the deformed geometry is [6]

$$\frac{1}{\rho_\theta} = \frac{1}{r^2}\left(\frac{\partial(\theta w)}{\partial\theta} + \frac{\partial^2 w}{\partial\theta^2}\right), \tag{9}$$

so that the azimuthal plastic bending energy dissipation rate is

$$\dot{\Gamma}_{az} = \frac{v}{a}\frac{\sigma_y h}{4}\int_0^a\int_{-\pi}^{\pi} r \, dz \, d\theta \frac{h}{\rho_\theta}$$

$$= \frac{\pi}{4}\left(1 + \frac{2}{\pi^2}\right) Bvra\left(\frac{h^2}{r^2}\right)\sigma_y. \tag{10}$$

The axial bending energy dissipation rate is calculated in a similar fashion. To a first approximation the axial radius of curvature is given by

$$\frac{1}{\rho_z} \approx \left|\frac{d^2 w}{dz^2}\right|, \tag{11}$$

which yields

$$\Gamma_{ax} = \int_0^a\int_{-\pi}^{\pi} \Gamma(z, \theta) r \, d\theta \, dz = \frac{\pi^2}{6}\sigma_y r h^2 B. \tag{12}$$

On advancing the crack by a length $a$, twice this work is done (in bending and unbending the cladding) so we have

$$\dot{\Gamma}_{ax} = \frac{\pi^2}{3}\sigma_y \frac{rvh^2 B}{a}, \tag{13}$$

giving a total plastic dissipation rate of $\dot{\Gamma} = \dot{\Gamma}_{ax} + \dot{\Gamma}_{az}$.

We now consider how elastic bending-unbending can alter the magnitude of $\dot{\Gamma}_{ax}$. This is controlled by the magnitude of $B$: if $B$ is small enough then the radius of curvature is large enough everywhere so as never to produce any plastic bending. The analysis is lengthy, but eventually gives a generalisation of eq. (13):

$$\dot{\Gamma}_{ax} = \frac{\pi^2}{3}\sigma_y \frac{rvh^2 B}{a} C(\phi),$$

$$= \frac{\pi^2}{3}\sigma_y \frac{rvh^2 B}{a}\left((1-\phi^2)^{1/2}\right.$$

$$- \frac{6}{\pi}\phi \cos^{-1}\phi\left(1 - \frac{4}{3}\phi^{1/2}\left(1 + \tfrac{1}{12}(\cos^{-1}\phi)^2\right)\right)$$

$$\left. - \frac{3}{\pi}\phi^2 \ln\left[\frac{1}{\phi}\left(1 + (1-\phi^2)^{1/2}\right)\right]\right), \tag{14}$$

where

$$\phi = \frac{4a\sigma_y}{hE\pi^2 B}. \tag{15}$$

The previous result is obtained at $\phi = 0$. For $\phi \geq 1$, $C(\phi) = 0$. We shall shortly discuss an upper limit for $B$ which implies that $\phi \geq \epsilon_e/\epsilon_f$, where $\epsilon_e$ and $\epsilon_f$ are the elastic and plastic fracture strains respectively, and so $\phi \geq 0.1$. Figure 2 illustrates the behaviour of the correction function $C(\phi)$, which suggest that $\dot{\Gamma}_{ax}$ in eq. (13) should be reduced by 20–30%.

Finally we consider a third process of energy dissipation, that required to bring new cladding into motion at the crack tip zone. It is considered that such energy

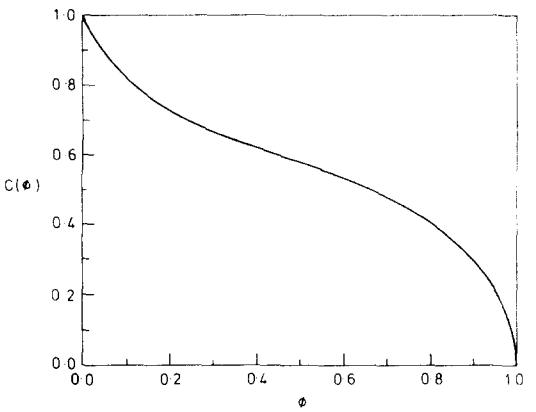

Fig. 2. Axial plastic bending correction factor.

is not returned to the accelerating material (in $0 < z < a/2$) by those parts which are decelerating (in $a/2 < z < a$). This kinetic energy is lost in other ways, possibly in elastic straining behind the crack tip, which does not feed back to the crack tip region.

The kinetic energy dissipation rate is

$$\dot{T}_K = \frac{v}{a}\int_0^a\int_{-\pi}^{\pi} r\,\mathrm{d}z\,\mathrm{d}\theta\tfrac{1}{2}\rho_c\dot{w}^2 h = \frac{\pi^3}{40}\rho_c h r B^2 v^3, \qquad (16)$$

where $\rho_c$ is the cladding density. Note that this term is proportional to $v^3$ whilst previous energy flow rates were proportional to $v$. Because of this we can determine an equation for the velocity, using a straightforward steady-state energy balance equation:

$$\dot{W} + \dot{A} = \dot{T}_K + \dot{F} + \dot{\Gamma}. \qquad (17)$$

We first consider some of the features of this equation. In the limit of no deformation, $B \to 0$ and eq. (17) becomes $\dot{A} = \dot{F}$ which is equivalent to the Griffith criterion for the extension of a brittle crack [11]:

$$\frac{\partial A}{\partial z} > \frac{\partial F}{\partial z}. \qquad (18)$$

However, a more careful treatment of the elastic energy supply rate, with a consideration of the elastic stress and strain fields, would be necessary in order to provide a proper treatment of brittle crack propagation. Elastic effects have little importance in our situation, however, and the simplified approach is justified.

Secondly, we have neglected terms of order $B^2$ in the calculation of $\dot{\Gamma}_{ax}$, and yet now we propose to use it in eq. (18) where a $B^2$ term appears, namely $\dot{T}_K$. There is no inconsistency, however, since the $\dot{T}_K$ term is of the same absolute order of magnitude as the order $B$ term in $\dot{\Gamma}$: the equation should not be viewed simply as having been expanded in the parameter $B$.

In order to proceed we still need to specify the deformed geometry completely, through the parameters $a$ and $B$. Once again, an elasto-plastic stress–strain solution for the system would presumably provide these as functions of the dimensions of the cladding and the driving pressure, but in the absence of a solution we have to provide good estimates.

The plastic deformation in the crack flaps gives an upper limit on $B$ corresponding to an axial bending strain at the clad inner and outer surfaces, at the edges of the crack, just equal to the fracture strain $\epsilon_f$, as the clad is forced through its S shape. We shall use this limit to fix $B$ (though it should be recognised to be merely an upper limit):

$$B = \frac{4a(\epsilon_f + \sigma_y/E)}{h\pi^2}. \qquad (19)$$

In actual fact, this condition should be exploited as a criterion for the fragmentation of the clad by the formation of secondary cracks as the rupture occurs, an area which is being pursued, and $B$ should be determined in another way. Using eq. (19), the velocity is now obtained from eq. (17) as follows:

$$v^2 = \frac{10}{3\rho_c(\epsilon_f + \sigma_y/E)} \times\left[P - \frac{\sigma_y h}{r}\left(\frac{\pi r h}{a^2}C(\phi) + \frac{3h}{4r}\left(1 + \frac{2}{\pi^2}\right)\right) + \frac{3h\pi^2(\sigma_\theta^2 - K^2/\pi r)}{4rE(\epsilon_f + \sigma_y/E)}\frac{hr}{a^2}\right]. \qquad (20)$$

Since eq. (19) is only an upper limit on $B$, this should be regarded as a lower limit on $v$.

The last unknown parameter is the crack tip length $a$. Maxey et al. [14,15] have analysed crack propagation data in gas pipelines and have proposed an "equivalent crack length" $c$ equal to $3(rh)^{1/2}$ for a propagating crack. This conclusion is based on a static energy analysis of a crack tip of length $c$: instability with respect to extension occurs if

$$\frac{8}{\pi}\sigma_y^2 c\,\ln\left[\sec\left(\frac{\pi}{2}(1 + 1.61c^2/(rh))\frac{\sigma_\theta}{\sigma_y}\right)\right] \geq K^2. \qquad (21)$$

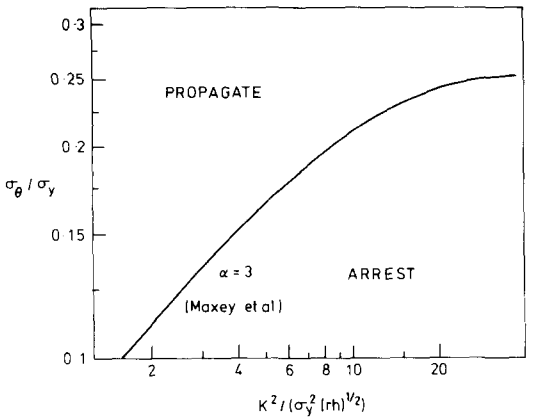


Fig. 3. Arrest and propagate regions of gas pipeline crack behaviour.

This result is a generalisation of the brittle crack extension condition, $\sigma_\theta(\pi c)^{1/2} \geq K^2$ [11], to allow for small scale plasticity in the crack tip region [12,13]. It is derived on the basis of small scale yielding, but remains approximately true even for $\sigma_\theta/\sigma_y$ as large as 0.9. The left hand side of eq. (21) is proportional to the elastic energy release rate upon increasing $c$; the right hand side the fracture energy dissipation rate. A simple assumption is to write a dimensionless $c = \alpha(rh)^{1/2}$ whereupon the instability criterion for $\alpha$ is

$$f\left(\alpha, \frac{\sigma_\theta}{\sigma_y}\right) = \frac{8\alpha}{\pi} \ln\left[\sec\left(\frac{\pi}{2}(1 + 1.61\alpha^2)\frac{\sigma_\theta}{\sigma_y}\right)\right] \geq \frac{K^2}{\sigma_y^2(rh)^{1/2}}. \tag{22}$$

Maxey and collaborators studied gas pipeline crack propagation data on a plot of $\sigma_\theta/\sigma_y$ against $K^2/(\sigma_y^2(rh)^{1/2})$ and found that a function of the form in eq. (22) could separate regions of crack arrest from crack propagation, using a value $\alpha = 3$. This is illustrated in fig. 3 and the details are given more fully in the original literature [14,15,16]. The implication is that a running ductile crack tip shows some resemblance to a static crack with a constant crack tip length $c = 3(rh)^{1/2}$. Stress and fracture toughness conditions for either continued quasi-stable propagation, or crack arrest, are then described by eq. (22) with $\alpha = 3$, and illustrated by the two regions in fig. 3.

We now identify the static crack tip length $c$ with the quasi-stable running crack tip length $a$ to give

$$a = 3(rh)^{1/2}, \tag{23}$$

a result which yields the velocity equation

$$v^2 = \frac{10}{3\rho_c(\epsilon_f + \sigma_y/E)} \times \left(P - \left(\frac{\pi}{9}C(\phi) + \frac{3}{4}\frac{h}{r}\left(1 + \frac{2}{\pi^2}\right)\right)\frac{h}{r}\sigma_y + \frac{h\pi^2(\sigma_\theta^2 - K^2/(\pi r))}{12rE(\epsilon_f + \sigma_y/E)}\right). \tag{24}$$

Although the above static analysis considered the relaxation of elastic strains around the crack tip, expressed as the left-hand side of eq. (21), during steady propagation the crack shape is constant, $c$ does not change, and so no elastic contribution to eq. (17) is missing. The $\dot{A}$ contribution considered earlier, the relaxation of elastic stresses corresponding to the previous uncracked geometry, with energy density $\sigma_\theta^2/(2E)$, is indeed the only contribution. The fracture energy change, represented in eq. (21) as the right-hand side, continues to apply during steady propagation, and appears in eq. (17) as the $\dot{F}$ term.

During ductile crack propagation $P \approx \sigma_y h/r$ and so it can be seen that plastic dissipation amounts to about 30–40% of the internal pressure work rate. Also, it is instructive to express the remaining terms in a similar manner. The elastic work rate in the brackets in eq. (24) can be written

$$\frac{h\pi^2\sigma_\theta^2}{12rE(\epsilon_f + \sigma_y/E)} = \frac{h\sigma_\theta}{r}\left(\frac{\pi^2\epsilon_e}{12(\epsilon_f + \epsilon_e)}\right) \approx 0.1P, \tag{25}$$

where $\epsilon_e$ is again a typical elastic strain. As for the fracture work term, the crack tip opening displacement (CTOD) is related to $K$ by

$$\text{CTOD} = \frac{K^2}{E\sigma_y}. \tag{26}$$

Let this displacement be a fraction $\beta$ of the maximum crack width $\pi\delta$. Then

$$\frac{h\pi^2K^2/\pi r}{12rE(\epsilon_f + \sigma_y/E)} = 3\beta\frac{\sigma_y h}{r}. \tag{27}$$

The geometry of real cracks would suggest that the circumferential displacement at the crack tip is much less than the total displacement after the crack has passed, and calculations to be presented later using actual data would correspond to $\beta \approx 1/12$.

In summary, the greatest contribution to the energy balance, apart from the internal pressure term, is the plastic axial bending term. This is in accordance with the conclusions of Freund and Parks [6], though several studies have ignored the plastic term [13,7].

We have now obtained an equation for the velocity of an axial cladding crack, which can be used to solve the equation $dZ/dt = v(Z)$ for each end of the rupture, with $Z$ the fuel pin axial coordinate, making due use of the axial, or $Z$, dependence of the various quantities in eq. (24), and therefore of $v$. What we need now is an initial condition $Z(t = 0)$ for each crack tip, and a termination condition for the propagation.

### 2.2. Crack nucleation

The question addressed here is not whether a crack forms, which is properly described by the failure criteria developed previously [1,2], but whether the crack so created will begin to propagate in the steady fashion we have assumed. This can be approached using arguments set out in the last section: for the particular conditions at the failure point, a static crack half-length $c_{crit}$ can be found corresponding to static instability, using eq. (21). If this statically unstable crack tip length is less than the steady state crack tip length $a$, then all is consistent. The crack will presumably be pushed over this critical size, become unstable and develop into the steady state geometry, with a larger crack tip length. If, however, $a$ is less than the static crack tip length required for instability, then the crack will never begin to run. This can be illustrated using fig. 3. Not only does the function $f(\alpha = 3, \sigma_\theta/\sigma_y)$ separate regions of parameter space where cracks run and where they arrest, but also the "arrest" region corresponds to conditions where the statically unstable initial crack tip length $c_{crit}$ is greater than $a = 3(rh)^{1/2}$. Thus fig. 3 has a dual role, illustrating criteria of nucleation and propagation.

For a cladding failure by the transgranular, plastic yield mechanism [1], where $\sigma_\theta \approx \sigma_y$, the value of $c_{crit}$ is very small and the crack will almost certainly propagate, subject to a real solution for $v$ from eq. (24). (In principle the energy dissipation may exceed the supply rate, implying $v = 0$. This is unlikely to occur in eq. (24), as one can see by replacing $\sigma_y h/r$ by $P$). For intergranular fracture, or when the cladding fails by some stress-unrelated mechanism such as by corrosion, $\sigma_\theta$ is not necessarily equal to $\sigma_y$ and the crack may not propagate. Such a crack would correspond to a pin-hole failure with a rupture area of small extent, around 1 $mm^2$.

The initial condition for the propagation, when it occurs, is taken to be $Z(t = 0) = Z_F \pm a$, for the upper and lower tips of the clad rupture, where $Z_F$ is the position of clad failure measured, say, from the bottom of the fuel column. This assumes that the steady state of propagation is set up immediately.

### 2.3. Crack arrest

In principle eq. (24) can describe crack arrest by the reduction of source terms, or the increase in sink terms, such as to reduce the right-hand side to zero. Crack arrest is achieved in the design of gas pipelines by inserting sections of pipe of a different material (with larger fracture toughness) at frequent stages so that a propagating crack in the main pipe will be unable to continue [16]. Equivalently, by having a more ductile pipe section in line, the plastic work term can be increased, through a reduction in $\phi$, thereby reducing or eliminating the propagation velocity. Such considerations do not enter greatly into cladding rupture calculations since material parameters and stress conditions do not typically show sufficient variation along the pin. This is analogous to a gas pipeline without crack arrestor sections, where accidental pipe ruptures have occasionally resulted in cracks propagating for very long distances: up to 8 miles (13 km) is recorded, though the fracture mode in this example was brittle [18].

An analysis of the process of gas escape from a steadily propagating crack can be done [6], showing that even if the propagation velocity is less than the gas sound velocity, a sizeable gas pressure can be maintained around the crack tip. The local pressure $P_l$ is related to the distant pressure $P$ by

$$P_l = P\left[\frac{2}{\gamma+1} + \frac{(\gamma-1)v}{(\gamma+1)c}\right]^{2\gamma/(\gamma-1)}, \tag{28}$$

where $c$ is the sound velocity in the gas and $\gamma$ is the ratio of the specific heat at constant pressure to that at constant volume, for the particular gas. For air, $\gamma \approx 1.4$. This steady state depressurisation can amount to a reduction of the driving pressure (and hoop stresses) to 28% of the initial failure pressure (for air), but in principle this could still be high enough to drive the crack, and indeed has done so in ductile gas pipeline rupture tests. If no arrestors are present, the only means of stopping the crack is the exhaustion of the source of gas in the pipe, terminating the steady state.

For cladding rupture the situation is made more complicated by the fission gas pressurisation of molten

fuel. If, during a reactor accident, the fuel melts, then the mobility of gases, generated by the fission of U or Pu, is greatly enhanced. Such a bubbly medium will behave differently to single phase gas, following rupture, and although some sort of local depressurisation at the running crack tips is likely (though not as great as in the gas case) it is difficult to estimate it. However, propagation is not expected to be terminated by the local crack tip depressurisation: in the fuel pin case it is almost certainly brought about by the exhaustion of internal pressure due to the finite extent of the molten fuel cavity inside the pin, and the expulsion of fuel from the pin. We shall concentrate on modelling this particular mode of pin pressurisation and rupture, though briefly we mentioned alternatives.

Firstly, fuel-clad mechanical interaction (FCMI) can cause high cladding stresses and clad failure. However, the pressurising internal medium is solid, and this responds in a qualitatively different manner following cladding rupture. The applied stresses are strain-limited far more strongly than when the pin is gas or molten fuel pressurised, due to the larger bulk modulus. This means that the assumption of constant $P$ across the deforming crack flaps is likely to be a poor one in eq. (1), and consequently the calculated $\dot{W}$ and the main driving force in the velocity equation are overestimates. An FCMI induced failure is therefore less likely to propagate than a molten fuel pressurisation case, given the same conditions. What is more, the applied internal pressure is more likely to be localised axially, leading again to a reduced chance of rupture propagation.

Secondly, fission gas pressurisation alone is a possibility, for instance in a circumstance where no fuel melting occurs. In principle, this situation is exactly the same as a gas pipeline analysis, and the same depressurisation approach could be used. Again, final arrest is likely to be due to fission gas exhaustion. It is likely that cracking driven by this mechanism would result in longer rips than for an equivalent molten fuel pressurised case. However, here we concentrate on the latter, more common, mechanism, leaving other situations for possible future development.

The model of depressurisation of the molten fuel cavity within the pin developed here is very simple and makes no attempt to treat the coupling between crack propagation and molten fuel behaviour, as it would greatly complicate the calculation. We prefer here to assume that a certain amount of molten fuel needs to be expelled from the pin, at which time the driving pressure is exhausted and the propagation ceases. The loss of pressure would occur smoothly but here we assume a sharp cut-off, and moreover that the initial pressure is unaffected up until this cut-off. Also, we neglect the possibility of a local crack tip reduction in pressure, analogous to the gas driven case, and indeed assume that for the purposes of calculating the expulsion rate of fuel, the pressure behind the crack is maintained at its initial level. The only test of these assumptions would be the comparison of predictions with experiments, which we shall come to later, but it is important to be aware of the approximations made.

The expulsion velocity of fuel through the rupture can be obtained using Bernoulli's equation:

$$v_e = (2P/\rho_f)^{1/2}, \tag{29}$$

where $\rho_f$ is the density of the molten fuel. The volume expelled at time $t$ after the pin rupture is given approximately by

$$\Delta V(t) = 2\int_0^t \left(\frac{2P}{\rho_f}\right)^{1/2} vt\pi\delta \, dt, \tag{30}$$

where $v$ is the crack velocity and $\delta$ the maximum radial displacement of the cladding. The local width of the crack is $\pi\delta$ and the length approximately $2vt$. $\delta$ can be found using eq. (19). Assuming constant $v$ and $\delta$, the expelled volume is then

$$\Delta V = (2P/\rho_f)^{1/2} v\pi\delta t^2. \tag{31}$$

In order to use this to provide an estimate of the arrest time $t_p$ we need to consider what $\Delta V$ is needed to depressurise the cavity. Figure 4 illustrates the melting, pressurisation, rupture and depressurisation of the

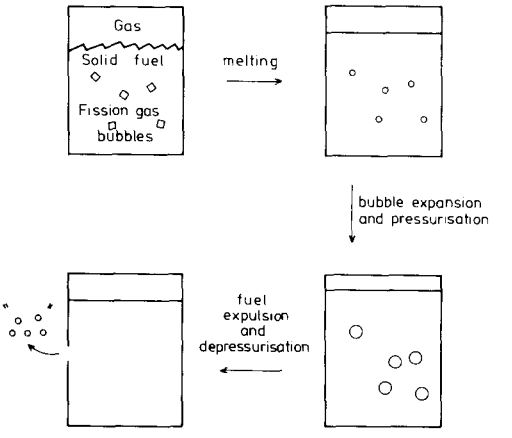


Fig. 4. Schematic sequence of melting, pressurisation and depressurisation of a molten fuel cavity.

cavity in simple terms. Melting reduces the restraint on fission gas bubbles in the fuel, allowing them to expand, which, together with the volume change of the fuel on melting is the underlying cause of the rise in internal pressure [19]. Clearly, the removal of a volume equal to that of the fission gas bubbles at pressure, $V_{BUB}$, would lead to a return to a situation similar to the initial state before melting (apart from the melting volume change). Of course, the expelled volume would in actual fact be a bubbly mixture of molten fuel and fission gas. Putting $\Delta V = V_{BUB}$ yields an expression for $t_p$ given by

$$t_p = \left[ \frac{V_{BUB}}{\pi v \delta} \left( \frac{\rho_f}{2P} \right)^{1/2} \right]^{1/2} . \tag{32}$$

Actually, $\Delta V$ refers to an expulsion volume measured outside the pin but we assume the expelled mixture is largely made up of (incompressible) fuel so that corrections for the pressure change can be neglected. If the driving pressure is increased, the depressurisation occurs more rapidly, by a combination of faster crack propagation ($v^2 \propto P$) and more rapid fuel expulsion. Indeed, this implies that the crack length, $2vt_p$, is approximately independent of driving pressure, a somewhat surprising result. The crack length is rather more importantly determined by the fission gas content of the molten fuel and suggests that cracks are likely to be longer for more highly irradiated fuel pins.

Equation (32) provides the crack arrest criterion which terminates the propagation. An estimate of the arrest time can be made. Using $\rho_f = 9000$ kg m$^{-2}$, $P = 20$ MPa, $v = 200$ m s$^{-1}$, $\delta = 0.3$ mm and $V_{BUB} = 2.5 \times 10^{-7}$ m$^3$ (all typical values) we obtain $t_p = 0.14$ ms, which is short compared with the timescales of other processes occurring. It is therefore justified to consider the rip propagation to be virtually instantaneous from a point of view of the other processes, so that system changes in temperatures or pressures, for example, can be ignored whilst the crack is opening. In the numerical model we have developed, rather than using eq. (32) directly to determine the arrest time, the total ejected volume is monitored by evaluating eq. (30) and arrest is signalled when this exceeds $V_{BUB}$.

Having now obtained models for each aspect of rip propagation: initial condition, crack tip velocities and an arrest criterion, we can use them in calculations to compare against experimental results.

### 2.4. Calculations

The gas pipeline studies mentioned earlier provide a useful database for testing the velocity model described above [15,16,20]. Tests were conducted on pipes of diameter about 1.2 m, both in the open and buried in the ground. An initial explosive charge initiated a crack, and the subsequent steady state propagation was observed. Assuming a suitable ductility of the steel, calculations of the crack velocity have been carried out using eq. (24) and are compared with experiment in table 1. There is reasonable agreement, considering the range of simplifying assumptions made, and the performance of the model is satisfactory.

Table 1
Gas pipeline crack propagation tests

| | British Gas tests ref. [16] | U.S. test SF 12W ref. [20] | U.S. test A31 (CA4) ref. [15] |
|---|---|---|---|
| $r$ (mm) | 610 | 530 | 460 |
| $h$ (mm) | 9.5 | 9.5 | 8.4 |
| $\rho_c$ (kg m$^{-3}$) | 8000 | 7770 | 7770 |
| $\sigma_\theta$ (MPa [a]) | 200 | 255 | 291 |
| $\sigma_y$ (MPa) | 383 | 531 | 484 |
| $\epsilon_f$ [b] | 0.02 | 0.02 | 0.02 |
| $K$ (MPa m$^{1/2}$) [c] | 219 | 335 | 335 |
| $v$ (expt) (m s$^{-1}$) | 125 m s$^{-1}$ | 244 | 260 |
| $v$ (calc) (m s$^{-1}$) | 151 m s$^{-1}$ | 176 | 222 |

[a] Locally decompressed hoop stress calculated using eq. (28), and $P = \sigma_\theta h / r$ assumed.
[b] Estimated ductilities.
[c] Toughness estimates from Charpy energies.

A computer code CRACKPRO has been written which integrates the equation of motion of each crack tip up to the arrest time. The axial variation of pin parameters is taken to be a linear interpolation between supplied data at a number of axial positions, so the calculation is over a continuous axial position variable $Z$. CRACKPRO calculates the value of the axial rip distance and the area of the rupture.

For the following illustrative calculations we use a fairly typical tube radius and wall thickness of 4 mm and 0.5 mm respectively. In the examples, cladding ductility, temperature and yield stress are taken to be axially constant, though this would certainly not be the case in real pin rupture experiments. Values of 0.02, 923 K and 300 MPa are taken respectively.

The fission gas content of the fuel can be estimated as follows. The number of gas atoms mobilised on the melting of the fuel is given by

$$n = (1 - f) \nu b \rho_f V_c / m \tag{33}$$

where $f$ is the fractional fission gas release from the fuel matrix, $\nu$ is the number of gas atoms generated

per fission, $b$ is the burn-up (the fraction of fissile atoms combusted), $\rho_f$ the fuel density, $V_c$ the molten fuel volume and $m$ the fissile atom mass. $V_{BUB}$ is then given by

$$V_{BUB} = \frac{nkT}{P} = (1-f)\frac{\nu b \rho_f V_c kT}{Pm}. \quad (34)$$

Using $f = 0.6$, $\nu = 0.28$, $\rho_f = 9000$ kg m$^{-3}$, $T = 3000$ K, $m = 4 \times 10^{-25}$ kg this gives

$$V_{BUB} = 2.6 \times 10^{-7}\left(\frac{b}{0.01}\right)\left(\frac{V_c}{5 \times 10^{-6}\ \mathrm{m}^3}\right) \times \left(\frac{20\ \mathrm{MPa}}{P}\right) \mathrm{m}^3, \quad (35)$$

where the characteristic molten fuel volume of $5 \times 10^{-6}$ m$^3$ assumes the whole of the fuel is molten over a pin length of 10 cm.

Figure 5 shows the crack length obtained for the above conditions as a function of $P$ for a burnup of 1%, and with $V_c = 5 \times 10^{-6}$ cm. The threshold at about 22 MPa, below which steady propagation as envisaged in the modelling is not possible, is very striking. Above this threshold, the crack length is not very sensitive to pressure. The timescales for the propagation are of the order of 0.1 ms.

Figure 6 shows the crack length as a function of burnup for a fixed $P$ of 30 MPa. For very low burnup, the depressurisation ought to be modelled with consideration given to the compressibility of molten fuel, since the amount of generated gas is low. The figure shows an increase in crack length as the fuel is more highly irradiated.

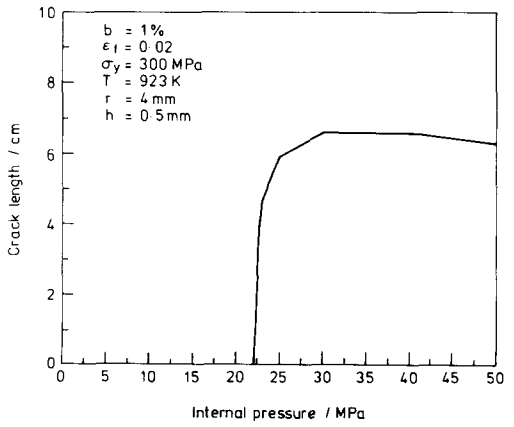


Fig. 5. Crack length against pin pressure.

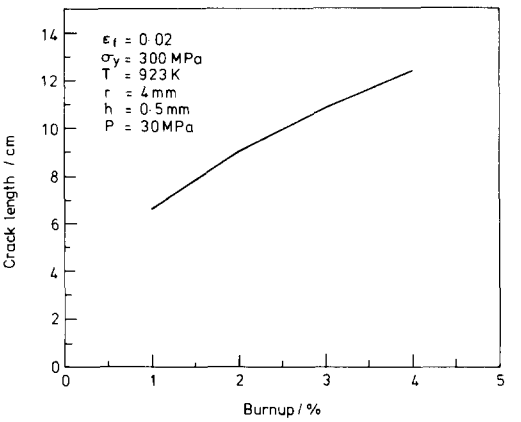


Fig. 6. Crack length against burnup.

Additional calculations have demonstrated such features of the model as the reduction in propagation with increased ductility. We now compare our calculations against real pin failure experiments. The A3 experiment was a transient overpower failure test of the CABRI-1 series [21] using a fresh pin initially at nominal operating conditions. Initial failure occurred 58 ms into the transient [22] and resulted in a rip extending across a region 47–51 cm according to fuel motion measurements, 45–48 cm according to coolant flow measurements, and 46–48 cm according to microphone measurements (all measurements made from the bottom of the fuel column (bfc) which was 75 cm long). The experiment was simulated using the TRAFIC fuel modelling code [19] incorporating the previously developed failure criteria [1,2], and the axial cracking process modelled using CRACKPRO. The result was a rip in the region 46.8–49.1 bfc at 58.2 ms, a length of 2.3 cm and an area of 0.038 cm$^2$. This good agreement is illustrated in fig. 7.

The BI2 experiment was also a transient overpower from CABRI-1, but from an initial state at an elevated temperature [22]. A 1% burnup pin was used. The initial rupture extended from 41.5–48.5 cm bfc and occurred at 79 ms. Figure 8 shows our predictions. Failure is predicted slightly early, but the extent of cracking is well accounted for. The rupture extended 7 cm and had an area of 0.8 cm$^2$. The greater extent than in the A3 test is accounted for by the fission gas present in the molten fuel.

## 4. Conclusions

We have sought to formulate mechanistic models of axial crack propagation in ruptured fuel pins. If soundly

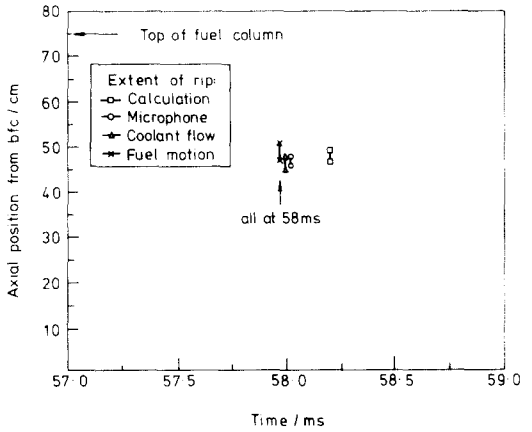


Fig. 7. Failure time, position and extent of rip in the A3 transient.

based, such models are likely to perform well in predicting the extent of cladding rupture in a variety of situations. A number of assumptions, simplifications and the neglect of particular effects have been made, since it has been our intention to construct an uncomplicated, easy to use numerical model for use in fuel pin and whole core modelling calculations. In this concluding section, we summarise the progress made and possible directions in which to develop the models further.

The rupture evolution mode we have concentrated on involves the propagation of a single axial crack away from the failure position. That is to say, no secondary cracks appear, and the ruptured geometry assumes the "open mouth" configuration illustrated in fig. 1. The tips of the crack are taken to assume a steady state

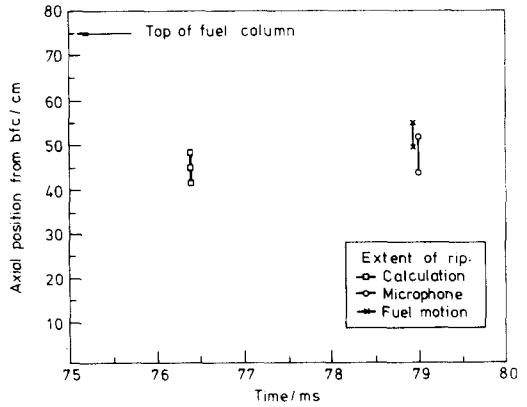


Fig. 8. Failure time, position and extent of rip in the BI2 transient.

shape within which all the deformation takes place: the material behind this region is then left in its deformed state. The actual geometry of the crack tips is based on some reasonable assumptions: a smoothly opening crack has been used, with the maximum radial displacement related to the crack tip length through a limit imposed by the cladding ductility. In actual fact, an elasto-plastic stress–strain solution to the problem ought to yield all geometric information, and the above limit should be used as a criterion for secondary cracking, and possible fragmentation of the cladding. This is one possible avenue for future development.

With the geometry given, the processes of energy supplies and losses can be analysed, with the result an expression for the crack propagation velocity. The difference between energy supplied by the work done by the internal pin pressure, plus any relaxed elastic stresses, against losses due to plastic dissipation and fracture surface creation, appears as the kinetic energy of accelerating clad material. The predictions of steady state crack velocities in several gas pipeline tests compare well against experiment.

Crack nucleation is indicated by material failure criteria, but a simple check is made on static instability under the prevailing conditions, to determine whether steady propagation is possible. A more detailed consideration is given to the process of pin depressurisation due to the exhaustion of material from within the pin, since this controls the arrest of the running crack. Depressurisation is expected to be most rapid if the fuel is solid (FCMI); for molten fuel pressurisation the process is slower, and for gas pressurisation, slowest of all. Crack lengths will increase in this order. We have considered molten fuel pressurisation as it is possibly the most common situation in fuel pin failures in conceptual accidents. The depressurisation interval is related to the fission gas content of the fuel so that for highly irradiated pins, the arrest times and resulting crack lengths are longer. The modelling is highly simplified, and some improvements could be made. The models describe the fracture of 20% cw AISI 316 stainless steel. However, since the models are based on generic physical processes, an extension to other materials is likely to involve simply changing the relevant material properties.

## Acknowledgements

This work was funded in part by the Commission of the European Communities, JRC Ispra, and in part by the Corporate Research Programme of AEA Technol-

ogy. Thanks are given to Robin Clement for help in constructing the numerical model.

## Nomenclature

| | |
|---|---|
| $a$ | crack tip length, |
| $b$ | burnup, |
| $B$ | shape parameter $\delta/a$, |
| $c$ | static critical crack tip length, |
| $C$ | plastic bending correction factor, |
| CTOD | crack tip opening displacement, |
| $E$ | Young's modulus, |
| $f$ | fission gas release fraction, |
| $\dot{F}$ | fracture work rate, |
| $h$ | clad wall thickness, |
| $K$ | fracture toughness, |
| $m$ | fissile atom mass, |
| $n$ | mobilised fission gas atoms, |
| $P$ | pin internal pressure, |
| $P_l$ | local pressure at clad tip, |
| $r$ | clad tube radius, |
| $t$ | time, |
| $t_p$ | depressurisation time, |
| $T$ | temperature, |
| $\dot{T}_K$ | kinetic energy dissipation rate, |
| $v$ | crack velocity, |
| $v_e$ | molten fuel ejection rate, |
| $v_{BUB}$ | volume of fission gas bubbles, |
| $V_c$ | volume of molten fuel, |
| $w$ | clad radial displacement, |
| $\dot{W}$ | work rate on clad from internal pressure, |
| $z$ | axial distance from crack tip, |
| $Z$ | axial distance from bottom of fuel column, |
| $Z_F$ | fracture position, |
| $\alpha$ | dimensionless crack length, |
| $\beta$ | CTOD/$\delta$, |
| $\gamma$ | ratio of specific heats, |
| $\Gamma(z, \theta)$ | plastic work density, |
| $\dot{\Gamma}$ | plastic work rate, |
| $\dot{\Gamma}_{ax}$ | axial plastic work rate, |
| $\dot{\Gamma}_{az}$ | azimuthal plastic work rate, |
| $\Delta V$ | volume of molten fuel expelled, |
| $\epsilon_e$ | elastic strain, |
| $\epsilon_f$ | ductility, |
| $\theta$ | azimuthal coordinate, |
| $\dot{\Lambda}$ | elastic energy release rate, |
| $\nu$ | gas atoms generated per fission, |
| $\rho$ | radius of curvature, |
| $\rho_c$ | clad density, |
| $\rho_f$ | fuel density, |
| $\rho_z$ | axial radius of curvature, |
| $\rho_\theta$ | azimuthal radius of curvature, |
| $\sigma_y$ | yield stress, |
| $\sigma_\theta$ | hoop stress, |
| $\phi$ | defined in eq. (15). |

## References


[1] I.J. Ford, J. Nucl. Mater. 182 (1991) 52.

[2] I.J. Ford, Intergranular fracture of irradiated stainless steel, Harwell report TP. 1347 (February 1990) to appear in Acta Metallurgica et Materialia.

[3] E.S. Folias, Int. J. Fracture Mech. 1 (1965) 104.

[4] F. Erdogan, M. Ratwani, Nucl. Eng. Design 20 (1972) 1.

[5] J. Sinclair, private communication.

[6] L.B. Freund, D.M. Parks, Analytical interpretation of running ductile fracture experiments in gas-pressurised linepipe, in: Crack Arrest Methodology and Applications, ASTM STP 711, G.T. Hahn and M.F. Kanninen, Eds. (1980) p. 359.

[7] W.A. Poynton, A theoretical analysis of shear fracture propagation in backfilled gas pipelines, British Gas/Institute of Gas Engineers Symposium: Crack Propagation in Pipelines, Newcastle, U.K., March 1974.

[8] F.H. Huang, G.L. Wire, Irradiation effects on the fracture toughness of 20% cold worked type 316 stainless steel, in: Dimensional Stability and Mechanical Behaviour of Irradiated Metals and Alloys (BNES, Brighton, 1983).

[9] D. Broek, H. Vlieger, The thickness effect in plane stress fracture toughness, Nat. Aerospace Inst. Amsterdam, TR-M-2152 (1965).

[10] D.P. Isherwood, J.G. Williams, The effect of stress-strain properties on notched tensile failure in plane stress, Eng. Fract. Mech. 2 (1970) 19.

[11] A.A. Griffith, Phil. Trans. Roy. Soc. of London, A221 (1921) 163.

[12] D.S. Dugdale, J. Mech. Phys. Solids 8 (1960) 100.

[13] G.T. Hahn, M. Sarrate, A.R. Rosenfield, Int. J. Fracture Mech. 5 (1969) 187.

[14] W.A. Maxey, J.F. Kiefner, R.J. Eiber, A.R. Duffy, Ductile fracture initiation, propagation and arrest in cylindrical vessels, ASTM STP 415 (1967) p. 25.

[15] W.A. Maxey, J.F. Kiefner, R.J. Eiber, A.R. Duffy, in: Proceedings of the 12th World Gas Conference, International Gas Union, Nice, France 1973, also summarised in ref. [16].

[16] G.D. Fearnehough, Fracture propagation control in gas pipelines: a survey of relevant studies, Int. J. Press. Ves. & Piping 2 (1974) 257.

[17] Anon. Oil & Gas Journal 58 (1960) 105.

[18] G.T. Hahn, M. Sarrate, M.F. Kanninen, A.R. Rosenfield, Int. J. Fracture 9 (1973) 209.

[19] I.J. Ford, R. Thetford, P. Edwards, N.P. Taylor, Mechanistic models of clad failure and molten fuel behaviour in the TRAFIC2 code and their application to transients,

Proc. International Fast Reactor Safety Meeting, Snowbird, Utah, August 1990.
[20] K.D. Ives, A.K. Shoemaker, R.F. McCartney, J. Eng. Mat. and Tech. 96 (1974) 309.
[21] G. Heusener, G. Kussmaul, D. Struwe, C. Cowking, J. Melis, F. Schmitz, J. Dadillon, A. Tattegrain, K. Takahashi, The CABRI Programmes - Motivations and Achievements, Proc. International Fast Reactor Safety Meeting, Snowbird, Utah, August 1990.
[22] D. Struwe, W. Pfrang, R. Cameron, M. Cranga, N. Nonaka, Fuel pin destruction modes – Experimental results and theoretical interpretation of the CABRI-1 programme, Proc. BNES Conference on Fast Reactor Core and Fuel Structural Behaviour, Inverness, 1990.